IEEE Photonics Journal
An IEEE Photonics Society Publication

Open Access

Indoor High Precision Three-Dimensional Positioning System Based on Visible Light Communication Using Improved Hybrid Bat Algorithm

Volume 12, Number 5, October 2020

Yong Chen
Han Zheng
Huanlin Liu
Zhaozhong Han
Zhimiao Ren

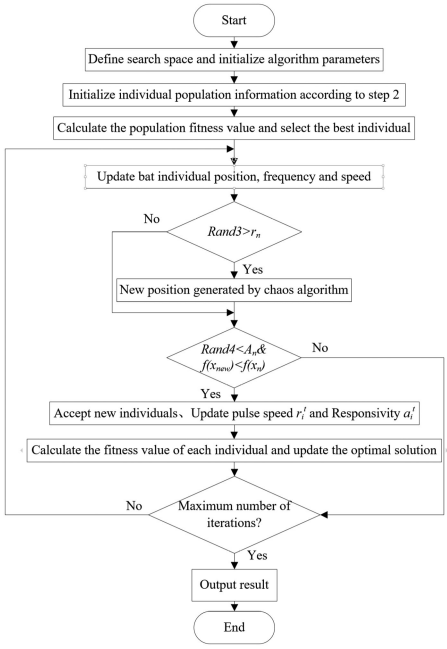

DOI: 10.1109/JPHOT.2020.3017670

Indoor High Precision Three-Dimensional Positioning System Based on Visible Light Communication Using Improved Hybrid Bat Algorithm

Yong Chen,[1] **Han Zheng**,[1] **Huanlin Liu**,[2] **Zhaozhong Han**,[1] **and Zhimiao Ren**[1]

[1]Key Laboratory of Industrial Internet of Things and Network Control, Ministry of Education, Chongqing University of Posts and Telecommunications, Chongqing 400065, China
[2]Key Laboratory of Optical Fiber Communication Technology, Chongqing University of Posts and Telecommunications, Chongqing 400065, China

DOI:10.1109/JPHOT.2020.3017670

Manuscript received July 19, 2020; revised August 11, 2020; accepted August 14, 2020. Date of publication August 18, 2020; date of current version September 15, 2020. This work was supported in part by the National Natural Science Foundation of China (51977021) and in part by the Science Foundation Project of Chongqing Science and Technology Commission (CSTC2019 jcyj-msxmX0613, cstc2020jcyj-msxmX0682), China. Corresponding author: Yong Chen (e-mail: chenyong@cqupt.edu.cn).
This article has supplementary downloadable material available at https://ieeexplore.ieee.org, provided by the authors.

Abstract: To solve problems of low positioning accuracy and long time-consuming in indoor visible light three-dimensional positioning system, a visible light three-dimensional positioning method based on the improved hybrid bat algorithm (IHBA) is proposed in this paper. Firstly, some beacon points are set at the beginning of the IHBA to reduce the number of iterations. Secondly, weight coefficient is defined to improve positioning accuracy when the fitness function is constructed. Thirdly, aiming at controlling the search speed reasonably, an adaptive search factor is introduced while the bat individual update formula is designed. Finally, the chaotic perturbation operation is used to avoid the algorithm falling into local optimum. In indoor simulation environment, the size of which is 5 m$\times$5 m $\times$ 3 m, the average positioning error of the IHBA is 1.16 cm and the positioning time is 1.85s. To verify the actual effectiveness of IHBA, a receiver is placed in the experimental environment, the size of which is 1.5 m $\times$ 1.2 m $\times$ 2 m. Through the optical power detected by the receiver, the processor calculate its coordinates with IHBA. The average positioning error of the IHBA is 3.64 cm and the positioning time is 0.89 s. The proposed algorithm has practical application value in existing indoor positioning methods.

Index Terms: Visible light communication (VLC), 3D positioning system, improved hybrid bat algorithm (IHBA).

1. Introduction

In recent years, location-based services have become a significant part of our daily lives. With the rapid development of wireless communication networks and mobile devices, the demand for accurate location-based services has been rising dramatically in many fields [1]. As a high-performance positioning system, GPS is widely used in outdoor positioning and navigation. However, it is difficult

for GPS to locate indoor targets with high precision because of the attenuation of satellite signal intensity and shadow effect.

At present, various indoor positioning system have been proposed,for example, Wi-Fi [2], Wlan [3], others positioning system [4]–[8] can satisfy the requirements of indoor positioning. However, visible light communication (VLC) positioning system is becoming a research hot owing to its low cost, low delay, high precision and anti-electromagnetic interference [9]–[12]. Positioning 3D static target and 2D fast moving target are hot research directions so far [13]–[16]. Meanwhile, positioning methods in VLC system include time-of-arrival (TOA), time-difference-of-arrival (TDOA), received signal strength (RSS), and angle-of-arrival (AOA) [17], [18]. RSS is chosen as our research object for its high positioning accuracy and low cost, which is also most widely investigated. Although numerous visible light three-dimensional (3-D) positioning algorithms have been proposed, some of them are still limited in application. In [19], the researchers used a single transmitter and multiple tilt optical receivers. On the one hands, this method requires a large number of devices, on the other hand, the limited power of LED makes it difficult to expand the positioning space. In [20], neural network algorithm were applied into visible light positioning (VLP) system, which selected the optimal number of hidden nodes to optimize the network. In [21], Deep learning model was used in VLP system. In [22], Xu proposed the VLP system based on location fingerprint method, but it is lack of experiment to support the idea. Based on ant colony algorithm [23], Wu integrated the error repair factor into it, and the positioning system achieved the positioning error within 4cm. In [24], the visible light positioning method based on improved genetic algorithm was proposed, which resulted in a large positioning delay. In reference [25], Wang proposed an indoor VLC three-dimensional positioning system based on immune algorithm. In [26], the visible light positioning method based on bat algorithm was proposed, which achieved the rapid positioning. In [27], the authors built a three-dimensional visible light positioning method based on chaotic particle swarm optimization. Meanwhile, the fitness function was constructed merely by using the spacing between the receiver and transmitter, which led to a reduction in positioning accuracy in the actual scene.

To solve the above problem, we propose an improved hybrid bat algorithm (IHBA). Firstly, some beacon points are set to participate in the construction of initialization population. Then, weight coefficient is defined to improve positioning accuracy in actual environment when the fitness function is constructed. Besides, the adaptive search factor is introduced to control the search speed reasonably. Finally, the chaotic perturbation operation is used to avoid the algorithm falling into local optimum.

The rest of the paper is organized as follows. In section 2, the indoor VLC positioning system model is introduced. In section 3, we discuss the IHBA in detail. In section 4, the simulation results of different methods are compared. In section 5, we present the experimental design and the results analysis of different algorithms. Finally, section 6 concludes the paper.

2. VLC System Model

The indoor visible light positioning system model is shown in Fig. 1(a), and the size of the room is 5 m $\times$ 5 m $\times$ 3 m. Four LEDs are evenly installed at the ceiling of the room and the coordinate of them are (1, 1, 3), (4, 1, 3), (4, 4, 3), (1, 4, 3) separately. Meanwhile, considering that the height of the general positioning equipment is about 1m, we selected three test points with a height of 1m. On this plane, point A is at the center, point B is at the edge, and point C is at the corner as the points to be located, which is used to test the positioning error of IHBA, and the coordinates of them are (2.5.2.5,1), (2.5,0.5,1), (4,4,1) separately.

Due to the long distance between LED and PD, LED can be regarded as Lambertian radiation source. Using the Lambertian radiation model, the channel gain $H(0)$ can be expressed as [28], [29]:

$$H(0) = \begin{cases} \frac{(m+1)A_{PD}}{2\pi {D_d}^2}\cos^m(\phi)\cos(\psi)g(\psi)T(\psi) & 0 \le \psi \le FOV \\ 0 & \psi > FOV \end{cases} \quad (1)$$

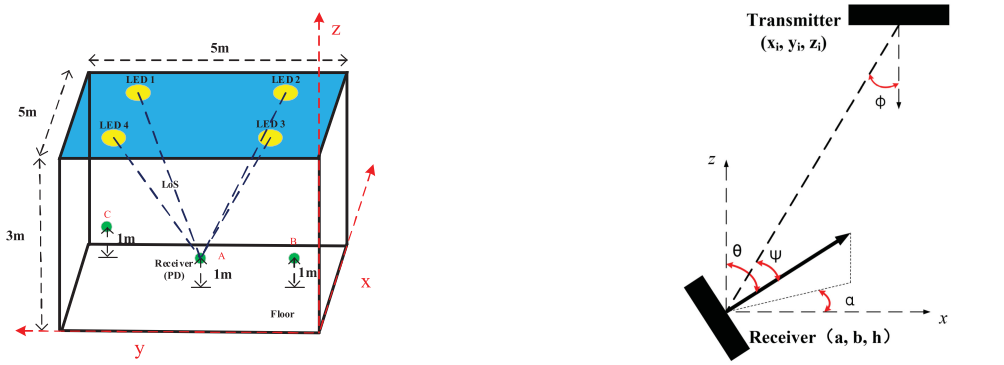

(a) Indoor VLC simulation scene (b) Tilt model of visible light communication

Fig. 1. Visible light positioning model.

where A_{PD} is the effective receiving area of PD, D_d is the distance between transmitter (i.e. LEDs) and receiver (i.e. PDs). ϕ and ψ represent the angle of irradiance and the angle of incidence respectively. *FOV* is the field of view of the receiver. $T(\psi)$ denotes the gain of the optical filter and $g(\psi)$ is the gain of the optical concentrator, and m is the Lambert index defined as:

$$m = -\frac{\ln 2}{\ln \cos \Phi_{1/2}} \tag{2}$$

where $\Phi_{1/2}$ is the angle at half illuminance of the transmitter. The gain of the optical concentrator $g(\psi)$ is defined as [30]:

$$\mathrm{g}(\psi) = \frac{n^2}{\sin^2(FOV)} \tag{3}$$

where n is the reflective index of a lens at PD. The optical power received by PD is calculated as follows:

$$P_r = P_t \times H(0) \tag{4}$$

where P_t represents the emitted power of the LEDs. In the VLC system, the noise component consists of shot noise ($\sigma^2{}_{shot}$), thermal noise ($\sigma^2{}_{therma}$) and inter symbol interference (P_{risi}) [31]. The quality of the received signal can be reflected by the signal-to-noise ratio (SNR), represented as

$$SNR = \frac{(RP_{rs})^2}{\sigma^2{}_{shot} + \sigma^2{}_{thermal} + (RP_{risi})^2} \tag{5}$$

where R represents the responsivity of the PD and P_{risi} is the average optical signal power received by the receiver.

Currently, the horizontal normal of the transmitter and receiver was aligned, and it also was perpendicular to the ceiling [32]. However, in actual environment, it is difficult to keep the transmitter and receiver parallel. The system model is built under considering the tilt of the receiver, as shown in Fig. 1(b). Then, the data calculated from the model is taken as the input of the algorithm to calculate the coordinates of the positioning points.

3. Improved Hybrid Bat Algorithm

In IHBA, beacon points are set at the beginning of the algorithm to reduce the number of iterations. Then the weight coefficient participates in the construction of fitness function to improve the accuracy in actual environment. Considering the traditional bat algorithm is poor in search ability, so we integrate the adaptive weighting factor, local frequency parameter and the chaotic algorithm into bat algorithm. The mapping relationship between hybrid bat algorithm and 3D positioning is shown in Table 1.

TABLE 1
Mapping Relationship Between Improved Hybrid Bat Algorithm and Three-Dimensional Positioning

Hybrid bat algorithm	Three-dimensional positioning problem
Fitness function	Positioning error and constraints
Bat individual	Possible positioning location
Fitness value assessment	Matching degree of feasible solution
Bat individual selection	Select the quality feasible solution
Global optimal bat individual	Optimal solution in the location search process

3.1 Initialize Parameters

The search space of IHBA is defined in the space of $L \times W \times H$, and the unit is meter. L, W and H represent the length, width and height of the space respectively. The position coordinates (x, y, z) of bats are constrained by three-dimensional space, which the range of x is$[0, L]$, y is$[0, W]$, and z is$[0, H]$. In the initialization of IHBA, there are N populations, individual loudness of bat is a, pulse emissivity is r. The maximum number of iterations is $t_{\max}$.

3.2 Initialize Population Individuals

The complexity and stability of the algorithm is related to the number of initialized individuals. At present, the first generation of population is often generated by means of randomly initialization in most literatures, such as [33] and [34]. This initialization method can easily lead to sparse and uneven distribution of individuals. In response to this problem, some beacon points are evenly set in the search space to guide the algorithm to quickly find the correct search direction at the early stage of the iteration. The coordinate of which can be noted $(\frac{1}{4}L, \frac{1}{4}W, \frac{1}{4}H)$,$(\frac{1}{4}L, \frac{3}{4}W, \frac{1}{4}H)$,$(\frac{3}{4}L, \frac{1}{4}W, \frac{1}{4}H)$,$(\frac{3}{4}L, \frac{3}{4}W, \frac{1}{4}H)$,$(\frac{1}{4}L, \frac{1}{4}W, \frac{3}{4}H)$,$(\frac{1}{4}L, \frac{3}{4}W, \frac{3}{4}H)$,$(\frac{3}{4}L, \frac{1}{4}W, \frac{3}{4}H)$, $(\frac{3}{4}L, \frac{3}{4}W, \frac{3}{4}H)$,$(\frac{1}{2}L, \frac{1}{2}W, \frac{1}{2}H)$.

Compared with the random distribution of all points during initialization [35], in the first iteration, all bat individuals are more likely to search in a better direction.

3.3 Fitness Function

According to the system model, most of the existing literatures [23]–[27] take the difference between the real distance of the location point and the estimated distance as the fitness function. Nevertheless, the fitness function constructed in the above literature does not consider the influence of the interference factors in the actual environment. Therefore, the weight coefficient w_i is used to construct fitness function F.

$$F = \sum_{i=1}^{4} w_i (D_i - d_i)^2 \tag{6}$$

$$w_i = \frac{\frac{1}{d_i}}{\frac{1}{d_1} + \frac{1}{d_2} + \frac{1}{d_3} + \frac{1}{d_4}} \tag{7}$$

where D_i is the true distance of the transceiver based on the coordinate difference, and d_i is the estimated distance of the transceiver based on the channel model.

3.4 Parameter Update

The performance of the IHBA is related to three parameters, which includes the position information of bats, velocity and frequency. The position update formula of the individual bat can be expressed as:

$$x_i^{t+1} = x_i^t + v_i^{t+1} \tag{8}$$

where x_i^t is the position of the *i-th* bat in the *t-th* iteration and v_i^{t+1} is the velocity of the *i-th* bat at the *(t+1)-th* iteration.

In order to control the flying direction of individual bats better, the local position information is introduced to update the speed. Q_{i1} and Q_{i2} is the frequency parameter controlling the local and global optimum flight direction respectively. For the sake of making the algorithm search quickly in the early stage and accurately in the later, adaptive weighting factor w_v, Q_{i1} and Q_{i2} are introduced to build the speed frequency update formula, as follows:

$$V_{i+1}^t = wV_i^t + rand1 * Q_{i1}(x_{pbest} - x_i^t) + rand2 * Q_{i2}(x_{gbest} - x_i^t)] \tag{9}$$

$$\begin{cases} Q_{i1} = Q_{1\max} - \frac{k(Q_{1\max} - Q_{1\min})}{t} \\ Q_{i2} = Q_{1\min} + \frac{k(Q_{1\max} - Q_{1\min})}{t} \end{cases} \tag{10}$$

$$w_v = w_{v\min} + (w_{v\max} + w_{v\min})S^{t-1} \tag{11}$$

where, V_{i+1}^t is the velocity of the *i-th* bat at the *t* iteration. and are the local and global optimum position. Meanwhile, *rand1* and *rand2* are two random numbers that produce differences between [0,1]. $w_{v\max}$ and $w_{v\min}$ are the maximum weight value and the minimum weight value, *S* is the attenuation value.

3.5 Disturbing Operation

In this paper, the chaotic logistic map is used to perturb the probability of the generated solution. Suppose *rand3* is a random number generated between sets [0,1], If *rand3* $> r_n$ is satisfied, the position coordinates of each new individual are mapped according to the following rules:

1) Generating chaotic sequence by chaotic logistic map$\{z_y | y = 1, 2, 3, \ldots, N\}$, chaos mapping is defined as:

$$\begin{cases} z_y = Rand() \\ z_{y+1} = \eta z_y(1 - z_y) \end{cases} \tag{12}$$

where, *Rand*() is the random number in the generation [0,1] interval, and η is the control factor of chaos factor controlling the intensity of chaos.

Generate the disturbance value corresponding to each individual, the operation is expressed as follows:

$$D(1:y) = 2(t_{\max} - t)Rand(1:y)/t_{\max} \tag{13}$$

where, *D* is the disturbance value generated, and $(1:y)$ represents *y* individuals from 1 to *y*.

1) Only the position coordinates of the new individual are disturbed, and the remaining parameters remain unchanged. The operation is expressed as follows:

$$pop_{new}(1:y) = p_{best}(1:y) - D(1:y) + 2D(1:y)z(1:y) \tag{14}$$

where, pop_{new} is the new individual after the disturbance.

3.6 Individual Selection Strategy

Suppose *rand4* is a random number in the interval of set [0,1], If *rand4*$>a_n$ and $f(x_{new})<f(x_n)$ are satisfied at the same time, the new solution generated by disturbing operation will be accepted. Then, the pulse response r_i^t and loudness a_i^t will be updated at the same time, the formula is defined as follows:

$$r_i^{t+1} = r_i^0(1 - e^{-\gamma t}) \tag{15}$$

$$a_i^{t+1} = \varepsilon a_n^t \tag{16}$$

TABLE 2
Simulation Model Parameters

Symbol	Parameters	Values
L×W×H	Room size	(5×5×3)m^3
	Position of LED1,LED,LED3,LED4	(1,1,3), (4,1,3), (4,4,3), (4,4,3)
H_{PD}	Receiving height	1m
P_t	Transmitted power of a lamp	5W
$\Phi_{1/2}$	Semi-angle at half power	30°
$T(\Psi)$	Gain of optical filter	1
A_{PD}	Physical area of photo-detector	1cm^2
n	Refractive index of lens at a PD	1.5
FOV	Field of view	60°
$g(\Psi)$	Gain of optical concentrator	1

TABLE 3
Simulation Algorithm Parameter

Symbol	Parameter	Value
Q_{1max}, Q_{2max}	Maximum frequency of individuals and populations	2.2
Q_{1min}, Q_{2min}	Minimum frequency of individuals and groups	0.2
N	Number of bat individuals in the population	30
t_{max}	Maximum number of iterations	100
S	Attenuation value	0.9
a	Individual loudness	0.6
r_0	Initial individual pulse emissivity	0.7
γ	Constant coefficient of pulse rate	0.9
v_{max}	Maximum speed limit	0.3
ε	Attenuation factor	0.9

where, r_i^{t+1} is the pulse loudness value of the *i-th* bat at the $t+1$ iteration, γ is the constant coefficient of pulse rate, a_i^{t+1} is the response value of the *i-th* bat at the $t+1$ iteration, and ε is the attenuation coefficient of loudness.

3.7 Iteration Termination Condition

In this paper, the maximum number of iterations is regarded as the termination condition of the algorithm. If the number of iterations does not reach the maximum number of iterations, repeat 3-6 until the number of iterations reach the maximum number of iterations.

4. Simulation Analysis

4.1 Feature Point Analysis

In Fig. 1, to prove the effectiveness of the IHBA algorithm, on the plane of 1m, center point A (2.5, 2.5, 1), edge point B (2.5, 0.5, 1) and corner point C (4, 4, 1) are selected to carry out the research. The simulation model and algorithm parameters of positioning system are shown in Tables 2 and 3 respectively. Fig. 2 shows the iterative state of the center position and the change of fitness function. The red point is the best individual in the current group and the blue point are candidates. The proposed algorithm converges at the 15th generation. We get the result of location point A was (2.5002, 2.4997, 0.9936) with error of 0.0065m. When the test point located at B, the algorithm converges at the 14th generation. The result of location point B of (2.5026, 0.5063, 1.0086) with location error is 0.011m. When the test point is located at C, the algorithm converges at the 18th

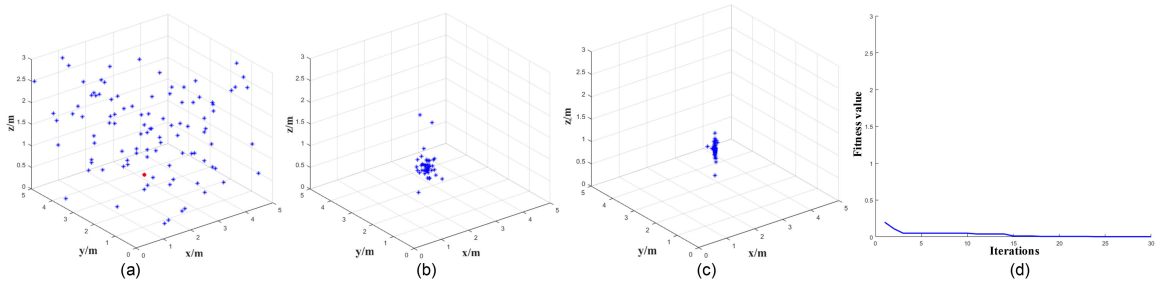

Fig. 2. The location point at the center of the room (2.5,2.5,1), use the IHBA algorithm iterative search in three-dimensional space. (a) The first generation of bat individual distribution. (b) The fifth generation of bat individual distribution. (c) The state of convergence. (d) The fitness convergence curve.

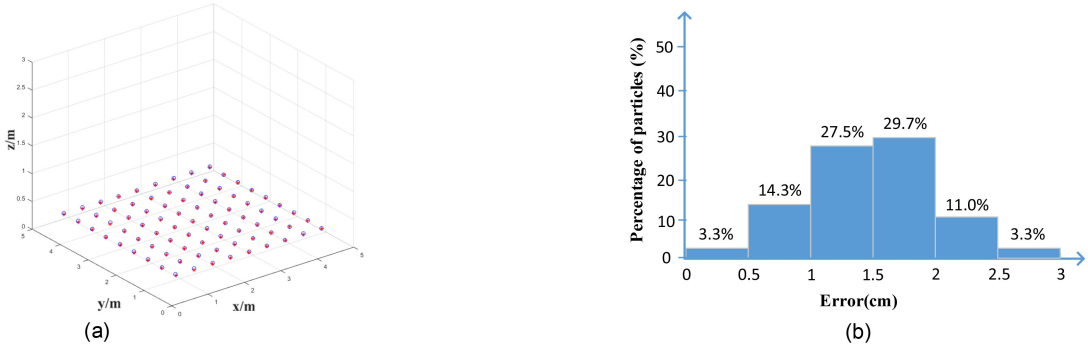

Fig. 3. (a) The positioning error map with a height of 0.3 m, where the red point is positioning estimate point and the blue point is positioning reference point. (b)The histogram of the error.

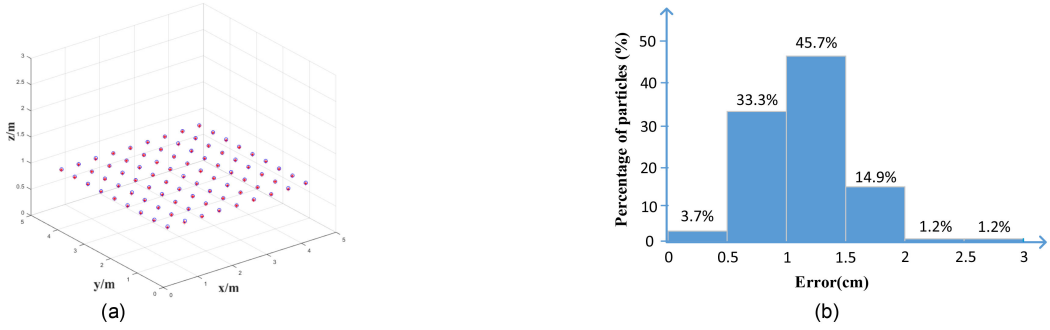

Fig. 4. (a) The positioning error map with a height of 0.9 m, where the red point is positioning estimate point and the blue point is positioning, (b) The histogram of the error.

generation. The result of location point C is (3.9964, 3.9968, 1.0055) with the location error of 0.0073 m.

4.2 Positioning Analysis at Different Heights

To test the overall positioning efficiency of the algorithm, as Figs. 3, 4, and 5 show, on the plane with height of 0.3 m, 0.9 m and 1.5 m, we select 81 positioning reference points evenly, whose interval is

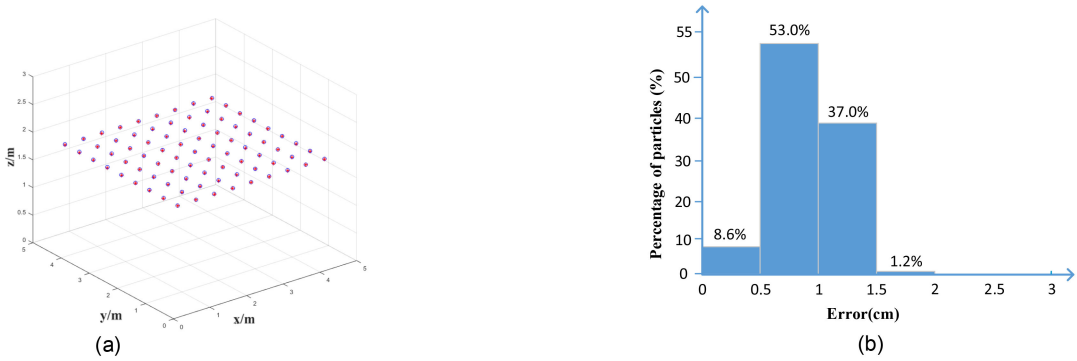

Fig. 5. (a) The positioning error map with a height of 1.5 m, where the red point is positioning estimate point and the blue point is positioning reference point. (b) The histogram of the error.

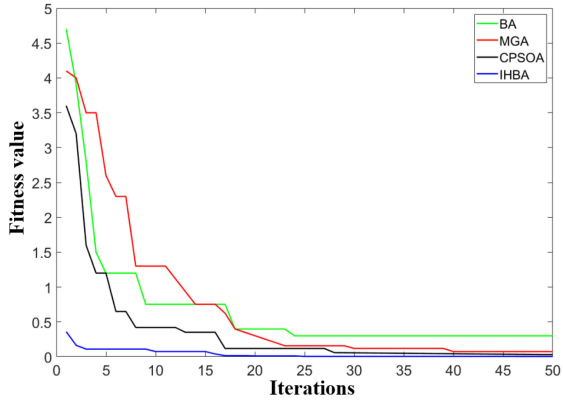

Fig. 6. Convergence of fitness values under IHBA, BA, and MGA.

TABLE 4
Results of the Different Algorithms

Algorithm	Number of iterations/ algebra	Iteration time/s	Average positioning error/cm	Maximum positioning error/cm	Minimum positioning error/cm
BA	24	3.58	6.23	8.12	3.48
MGA[24]	41	8.31	4.52	6.18	1.69
CPSO[27]	28	4.15	3.68	5.87	1.15
IHBA	16	1.85	1.16	2.85	0.38

0.5 m in length and width. The average positioning error on the corresponding plane are 1.48 cm, 1.17 cm, 0.83 cm respectively. Besides, the overall average positioning errors are 1.16cm.

To verify the performance advantage of our algorithm, bat algorithm (BA), modified genetic algorithm (MGA) [24], chaos particle swarm optimization algorithm (CPSOA) [27] and the improved hybrid bat algorithm (IHBA) are simulated in this paper. For fair, simulation are carried out in the same environment, including room size, LED position, power and so on. At the same time, 81 test points are selected on the plane with the height of 0.3 m, 0.9 m, and 1.5 m respect. A total of 243 test points participate in the test. Then, we set $N = 100$, $t_{\max} = 100$, each algorithm runs 30 times. The average is taken as final result. The change of fitness under different algorithms are shown in Fig. 6. Table 4 shows the positioning results under different algorithm. The comparison results

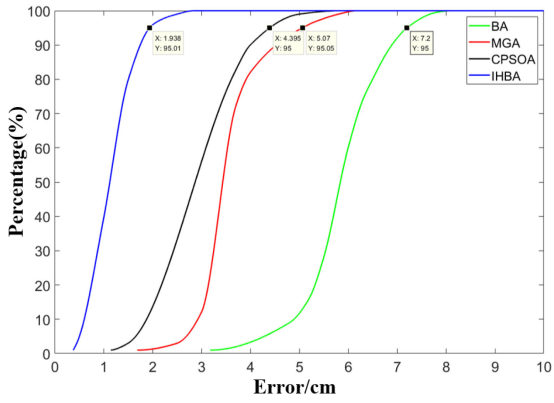

Fig. 7. Cumulative error distribution under IHBA, BA, MGA and CPSO algorithms.

show that the BA has a fast convergence speed and its convergence error is 6.23 cm at the 24th iteration. But the positioning accuracy of BA is low due to the problem of local optimal solution. The MGA converges at the 41st iteration with a positioning error of 4.52 cm, its accuracy of calculation is higher than BA. Yet it has a slow convergence speed. The CPSO algorithm converges at the 28th iteration with a positioning error of 3.68 cm, which is better than MGA algorithm in calculation speed and positioning accuracy. However, the IHBA proposed in this paper converges at the 16th iteration, with a positioning error of 1.16 cm. The speed of calculation and positioning accuracy are better than the other three algorithms compared. As we can see in Fig. 6, at the beginning of implementation, because of the role of beacon point, the algorithm proposed can quickly find the candidate solution with small fitness value at the first iteration. In this way, the number of previous iterations can be reduced effectively. For the algorithm, it improves the positioning accuracy and reduces the positioning time.Fig. 7 shows the accumulated distribution of positioning errors using four algorithms. It can be seen from the Figure that 95% of the positioning error of the algorithm proposed is within 1.938 cm, which is obviously superior to the algorithms of BA, MGA and CPSOA.

5. Experiments and Results Analysis

5.1 Experiment Building and Parameter Setting

To verify the effectiveness of the proposed algorithm in the real environment. As shown in Fig. 8(a), we built an indoor positioning system with the size of 1.5 m $\times$ 1.2 m $\times$ 2 m. Four LED luminaries were installed on the top of bracket. The LED coordinates were (0, 0, 2), (1.5, 0, 2), (1.5, 1.2, 2), (0, 1.2, 2) respectively. The specific experimental parameters are shown in Table 5.In experiment, PWM was chosen to send visible light information [36]. As show in Fig. 8(b), the four LEDs transmitted PWM wave with the duty cycle was 4%, 8%, 12% and 20% respectively. The DC switching power supply provided 12V voltage for LED, the multi-channel stabilized voltage power supply cooperates with STM32F407 single chip microcomputer to realize the modulation of LED optical signal. PIN photodiode circuit module was used as the receiver which received the photoelectric signal in the space. After the signal filtered by STM32 using Kalman filter[37], the IHBA was used to get the positioning coordinates.

In order to test the positioning error in the experimental system, three planes with the height of 0.45 m, 0.9 m and 1.35 m were selected at the interval of 0.45 m. In each plane, 42 experimental sites were evenly selected and the width and length intervals were 0.2m. A total of 126 test points participated in the test.

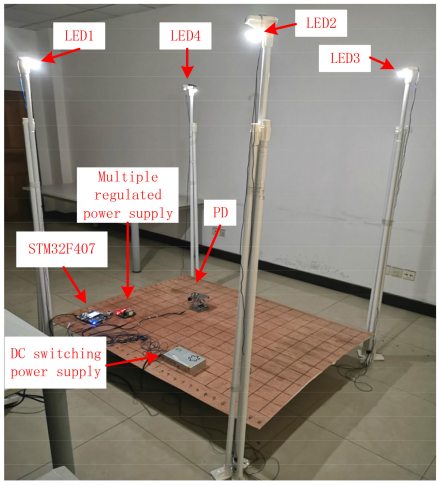

(a) Experimental platform of VLP system

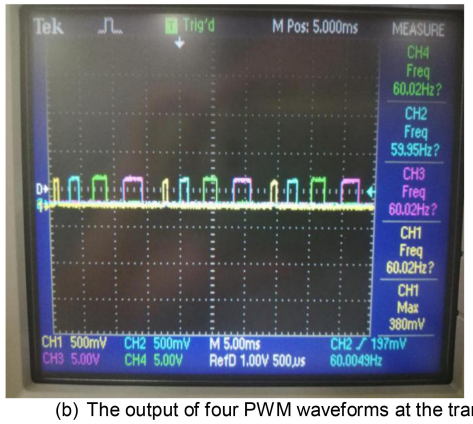

(b) The output of four PWM waveforms at the transmitter

Fig. 8. Visible light positioning experiment.

TABLE 5
System Model Parameters

Parameters	Values
Room size	1.5m×1.2m×2m
Position of LED1	(0,0,2)
Position of LED2	(0,1.2,2)
Position of LED3	(1.5,1.2,2)
Position of LED4	(1.5,0,2)
Transmitted power of a lamp	5W
Gain of optical filter	1
Physical area of photo-detector	$1cm^2$
Refractive index of lens at a PD	1.5
Field of view	60°
Gain of optical concentrator	1
Signal frequency	60Hz

5.2 Positioning Test and Results

In Fig. 9(a), (b) and (c) show the 3D positioning results at 0.45 m, 0.9 m and 1.35 m respectively. The red star point is the actual positioning coordinate point, and the blue circle point is the positioning coordinate point obtained by the algorithm.

The statistics of all test points in the three planes are shown in Fig. 10. As can be seen from the Figure, the positioning error of the visible light positioning system using the IHBA is mainly concentrated within 5 cm, accounting for about 88.9% of the total. The minimum positioning error is 0.88 cm, and the maximum one is 6.97 cm. The overall average error is 3.64cm. This result shows that IHBA has a better real location effect, reaching centimeter level.

Table 6 shows the mean value of plane positioning point error at the height of 0.45 m, 0.9 m and 1.35 m respectively. It can be analyzed from the data that the positioning error increases with the decrease of the height, which is consistent with the simulation results. Because the decrease of the height make the SNR of the receiver reduce, as a consequence of which, the positioning accuracy also decreases due to poor signal.

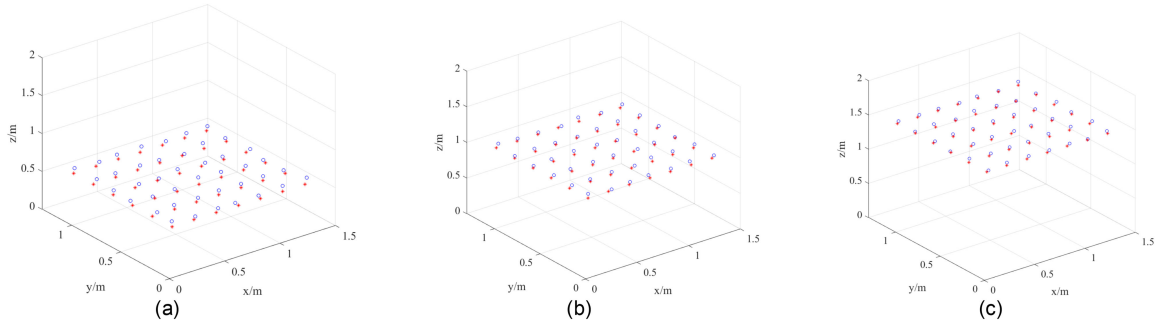

Fig. 9. (a)–(c) Experimental positioning results at the height of 0.45 m, 0.9 m, and 1.35 m.

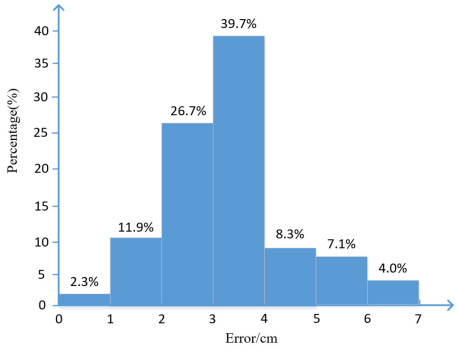

Fig. 10. Histogram of experimental positioning error distribution.

TABLE 6
Experimental Positioning Error

Height (m)	Error (cm)
0.45	4.76
0.9	3.28
1.35	3.15

TABLE 7
Results of the Four Algorithms Parameter

Algorithm	Iteration time/s	Average positioning error/cm	Maximum positioning error/cm	Minimum positioning error/cm
MGA[24]	2.98	6.47	10.2	4.3
CPSO[27]	1.76	5.59	8.34	3.45
IHBA	0.89	3.64	6.97	0.88

Then MGA and CPSO is compared with IBHA under the same experimental conditions. We reproduced the algorithm from the compared literature and keep other hardware facilities in the same. The distribution of test points is the same under different algorithm. The results are shown in Table 7.

Compared with the MGA and CPSOA, the performance of IHBA in accuracy and speed has been significantly improved. The positioning error of IHBA is reduced by 43.74% and 34.88% respectively. The time required for positioning in STM32F407 single chip processor is 0.89 s. Besides, the proposed algorithm takes less time to locate than the other two algorithms. It is shown that IHBA can show a better performance in positioning.

6. Conclusion

An indoor VLC three-dimensional positioning system based on improved hybrid bat algorithm (IHBA) is proposed in this paper, which improves the positioning precision and reduces the location time. Considering that PD has a large tilt probability, we build a sensor tilt model, further optimized it. Then, we use IHBA to calculate the optimal positioning solution in three-dimensional space and verify its performance. Moreover, we compare IHBA with the existing VLC three-dimensional positioning system. Simulation results show that the IHBA has higher positioning precision and shorter convergence time. Finally, an experimental system was built to prove the efficiency of the algorithm in actual scene, the size of which is 1.5 m $\times$ 1.2 m $\times$ 2 m. In the actual environment, the average positioning error of IHBA is 3.64 cm with calculation time of 0.89 s. The result shows that the proposed positioning system can be a promising solution for indoor positioning applications. In the next step, we will explore the indoor 3D target positioning method considering the moving speed.

Acknowledgment

It will be sincerely appreciated to anonymous reviewers for their valuable comments and suggestions on this paper. Thanks for your kindly review.

References

[1] L. U. Khan, "Visible light communication: Applications, architecture, standardization and research challenges," *Digit. Commun. Netw.*, no. 2, pp. 78–88, 2017.
[2] Q. Liang and M. Liu, "An automatic site survey approach for indoor localization using a smartphone," *IEEE Trans. Automat. Sci. Eng.*, vol. 17, no. 1, pp. 191–206, Jan. 2020.
[3] M. Zhou, Y. Liu, Y. Wang, and Z. S Tian, "Anonymous crowdsourcing-based WLAN indoor localization," *Digit. Commun. Netw.*, no. 4, pp. 226–236, 2019.
[4] R. Carotenuto, M. Merenda, D. Iero, and F. G. Della Corte, "An indoor ultrasonic system for autonomous 3-D positioning," *IEEE Trans. Instrum. Meas.*, vol. 68, no. 7, pp. 2507–2518, Jul. 2019.
[5] K. Xu and Y. Ou, "Theoretical and numerical characterization of a 40 Gbps long-haul multi-channel transmission system with dispersion compensation," *Digit. Commun. Netw.*, vol. 1, no. 3, pp. 222–228, 2015.
[6] A. Tzitzis *et al.*, "Localization of RFID tags by a moving robot, via phase unwrapping and non-linear optimization," *IEEE J. Radio Freq. Identification*, vol. 3, no. 4, pp. 216–226, Dec. 2019.
[7] D. Feng, C. Wang, C. He, Y. Zhuang, and X. Xia, "Kalman filter based integration of IMU and UWB for high-accuracy indoor positioning and navigation," *IEEE Internet Things J.*, vol. 7, no. 4, pp. 3133–3146, Apr. 2020.
[8] M. S. A. Mossaad, S. Hranilovic, and L. Lampe, "Visible light communicationsusing OFDM and multiple LEDs," *IEEE Trans. Commun.*, vol. 63, no. 11, pp. 4304–4313, Nov. 2015.
[9] H. H. Yin, Y. Q. Dong, Q. Zou, "Design and implementation of a visible light communication system in mobile scene," *J. Chongqing Univ. Posts Telecommun. (Natural Sci. Ed.)*, vol. 29, no. 04, pp. 487–493, 2017.
[10] K. Xu, "Silicon MOS optoelectronic micro-nano structure based on reverse-biased PN junction," *Physica Status Solidi (a)*, vol. 216, no. 7, 2019, Art. no. 1800868.
[11] J. Zhang and H Wang, "An improved optimization method of SNR uniformity in visible light communication system," *J. Chongqing Univ. Posts Telecommun. (Natural Sci. Ed.)*, vol. 27, no. 1, pp. 78–82, 2015.
[12] C. G. Ye, R. H Feng, and L. H. Mao, "A new visible radio frequency identification tag system with ACO-OFDM modulation," *J. Chongqing Univ. Posts Telecommun. (Natural Sci. Ed.)*, vol. 31, no. 01, pp. 72–79, 2019.
[13] W. Guan, X. Zhang, Y. Wu, Z. Xie, J. Li, and J. Zheng, "High precision indoor visible light positioning algorithm based on double LEDs using CMOS image sensor," *Appl. Sci.*, vol. 9, no. 6, 2019, Art. no. 1238.
[14] W. Guan, S. Chen, S. Wen, Z. Tan, H. Song, and W. Hou, "High-accuracy robot indoor localization scheme based on robot operating system using visible light positioning," *IEEE Photon. J.*, vol. 12, no. 2, Apr. 2020, Art. no. 7901716.
[15] J. Fang *et al.*, "High-speed indoor navigation system based on visible light and mobile phone," *IEEE Photon. J.*, vol. 9, no. 2, Apr. 2017, Art. no. 8200711.
[16] P. Lin *et al.*, "Real-time visible light positioning supporting fast moving speed," *Opt. Express*, vol. 28, no. 10, 2020, Art. no. 14503.
[17] M. F. Keskin, S. Gezici, and O. Arikan, "Direct and two-step positioning in visible light systems," *IEEE Trans. Commun.*, vol. 66, no. 1, pp. 239–254, Jan. 2018.
[18] S. Juneja and S. Vashisth, "Indoor positioning system using visible light communication," in *Proc. Int. Conf. Comput. Commun. Technol. Smart Nation (IC3TSN)*, 2017, pp. 79–83.
[19] S. H. Yang, H. S. Kim, Y. H. Son, and S. K Han, "Three-dimensional visible light indoor localization using AOA and RSS with multiple optical receivers," *J. Lightw. Technol.*, vol. 32, no. 14, pp. 2480–2485, Jul. 2014.
[20] A. G. Itziar, S. R. David, L. B. Carlos, and Q. A. Miguel, "Discrete indoor three-dimensional localization system based on neural networks using visible light communication," *Sensors*, vol. 18, no. 4, pp. 1040–1057, 2018.

[21] X. Lin and L. Zhang, "Intelligent and practical deep learning aided positioning design for visible light communication receivers," *IEEE Commun. Lett.*, vol. 24, no. 3, pp. 577–580, Mar. 2020.
[22] S. W. XU, Y. Wu, and X. F Wang, "Visible light localization algorithm based on sparsity adaptive and position fingerprint," *Acta Optica Sinica*, pp. 1–17, 2020.
[23] X. B. Wu, S. S. Wen, and J. Hua, "High precision 3D positioning system of indoor visible light based on ant colony algorithm," *J. Photon.*, vol. 46, no. 12, pp. 175–188, 2017.
[24] H. Chen, W. P. Guan, S. M. Li, and Y. X. Wu, "Indoor high precision three-dimensional positioning system based on visible light communication using modified genetic algorithm," *Opt. Commun.*, vol. 413, pp. 103–120, 2018.
[25] P. F. Wang, W. P. Guan, S. S. Wen, Y. J. Xie, Y. X. Wu, and M. Q. Zhang, "High precision indoor visible three-dimensional positioning system based on immune algorithm," *Acta Optica Sinica.*, vol. 38, no. 10, pp. 1–11, 2018.
[26] L. Huang, P. Wang, Z. Liu, X. Nan, L. Jiao, and L. Guo, "Indoor three-dimensional high-precision positioning system with bat algorithm based on visible light communication," *Appl. Opt.*, vol. 58, pp. 2226–2234, 2019.
[27] M. Zhang *et al.*, "A three-dimensional indoor positioning technique based on visible light communication using chaotic particle swarm optimization algorithm," *Optik*, vol. 165, pp. 54–73, 2018.
[28] X. Kaikai, "Silicon MOS optoelectronic micro-nano structure based on reverse-biased PN junction," *Physica Status Solidi*, vol. 216, no. 7, pp. 1800861–1800868, 2019.
[29] P. Chvojka, S. Zvanovec, P. A. Haigh, and Z. Ghassemlooy, "Channel characteristics of visible light communications within dynamic indoor environment," *J. Lightw. Technol.*, vol. 33, no. 9, pp. 1719–1725, 2015.
[30] M. Yasir, S.-W. Ho, and B. N. Vellambi, "Indoor positioning system using visible light and accelerometer," *J. Lightw. Technol.*, vol. 32, no. 19, pp. 3306–3316, 2014.
[31] Q.-L. Li, J. Y. Wang, T. Huang, and Y. J. Wang, "Three-dimensional indoor visible light positioning system with a single transmitter and a singer tilted receiver," *Opt. Express.*, vol. 55, no. 10, pp. 1–7, 2016.
[32] L. C. Mathias, L. F. D. Melo, and T. Abrao, "3-D localization with multiple LEDs lamps in OFDM-VLC system," *IEEE Access*, vol. 7, pp. 6249–6261, 2018.
[33] Y. Cai, W. P. Guan, Y. X. Wu, C. Y. Xie, Y. R. Chen, and L. T. Fang, "Indoor high precision three-dimensional positioning system based on visible light communication using particle swarm optimization," *IEEE Photon. J.*, vol. 9, no. 6, Dec. 2017, Art. no. 7908120.
[34] Y. Wu, Y. Xian, W. Guan, X. Chen, Q. Peng, and B. Chen, "High-precision indoor three-dimensional localization scheme based on visible light communication using modified fruit fly optimization algorithm," *Opt. Eng.*, vol. 57, no. 6, pp. 1–11, 2018.
[35] G. Yildizdan and ÖK. Baykan, "A novel modified bat algorithm hybridizing by differential evolution algorithm," *Expert Syst. with Appl.*, vol. 141, 2020, Art. no. 112949.
[36] Z. Cui, Y. Cao, X. Cai, J. Cai, and J. Chen, "Optimal LEACH protocol with modified bat algorithm for big data sensing systems in Internet of Things," *J. Parallel Distr. Com.*, vol. 132, pp. 217–229, 2019.
[37] C. Y. Lu, S. Wu, C. X. Jiang, and J. Hu, "Weak harmonic signal detection method in chaotic interference based on extended Kalman filter," *Digit. Commun. Netw.*, no. 1, pp. 51–55, 2019.